Search for the Standard Model Higgs Boson in the $ZH \to \mu^+\mu^- b\bar{b}$ Final State Using 7.9 fb^{-1}

The CDF Collaboration
http://www-cdf.fnal.gov
July 12, 2011

Abstract

We present a search for the Standard Model Higgs Boson using the process $ZH \to \mu^+\mu^- b\bar{b}$. We use a dataset corresponding to 7.9 fb^{-1} of integrated luminosity collected with the CDF II detector. This analysis benefits from several new multivariate techniques that have not been used in previous analyses at CDF. We use a multivariate function to select muon candidates, increasing signal acceptance while simultaneously keeping fake rates small. We employ an inclusive trigger selection to further increase acceptance. To enhance signal discrimination, we utilize a multi-layer approach consisting of expert discriminants. This multi-layer discriminant method helps isolate the two main classes of background events, $t\bar{t}$ and Z+jets production. It also includes a flavor separator, to distinguish light flavor jets from jets consistent with the decay of a b-hadron. With this novel multi-layer approach, we proceed to set limits on the ZH production cross section times branching ratio. For a Higgs boson with mass 115 GeV/c^2, we observe (expect) a limit of 10.2 (6.0) times the Standard Model prediction.

Preliminary Results

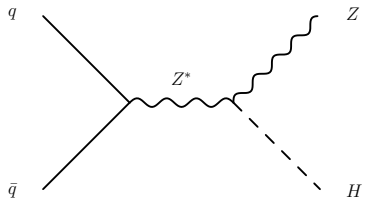

Figure 1: The Feynman diagram representation of the ZH associated Higgs production process.

1 Introduction

The last remaining particle predicted by the Standard Model but not yet observed is the Higgs boson. The Higgs boson is postulated to arise due to the spontaneous breaking of the $SU(2)\otimes U(1)$ symmetry of the Standard Model [1]. This spontaneous symmetry breaking gives mass terms to the appropriate particles in the Standard Model. Finding evidence for the Higgs boson would give more insight into electroweak symmetry breaking and the origin of mass in the Standard Model.

Many previous searches for the Higgs boson have been performed, and the allowed mass range continues to narrow. Experiments at LEP have excluded a Higgs boson with mass below 114.4 GeV/c^2 at the 95 percent confidence level [2]. The Tevatron experiments, CDF and D0, also have excluded a range of Higgs boson masses, $158 < m_H < 173$ GeV/c^2 [3], as well as $100 < m_H < 109$ GeV/c^2 [4], also at the 95 percent confidence level. In addition to direct searches from the aforementioned experiments, the other electroweak parameters of the Standard Model can be used to fit for the value of the Higgs mass. The latest fit result, which includes the experimental search results, is $m_H = 120.6^{+17.9}_{-5.2}$ GeV/c^2, where the errors represent the 1-sigma deviations[5].

In this analysis, we use the ZH associated production channel, as seen in the Feynman diagram in Figure 1. The ZH channel is best for searches in the low-mass regime, $100 < m_H < 150$ GeV/c^2. In this regime, the Higgs boson has a high branching ratio to $b\bar{b}$ pairs, and we utilize this property by searching for jets consistent with the decays of long-lived b-hadrons. The leptons from the decay of the Z boson help reduce QCD background processes. We search for events with two muons consistent with the decay of a Z boson and two or more jets, with additional requirements to identify decays of b quarks. This analysis is complementary to a similar analysis which uses the $ZH \to e^+e^-b\bar{b}$ final state[6]. Many of the advanced analysis techniques are shared between these two channels.

In this note, we detail our analysis methods, especially the novel multivariate techniques which are used for signal discrimination. We proceed to report our results in the form of expected and observed limits on the ZH production cross section times branching ratio for the $H \to b\bar{b}$ process.

2 Event Selection

We search for events using data collected with the CDF II detector, corresponding to an integrated luminosity of 7.9 fb^{-1}. We utilize two independent sets of triggers ('streams'), one which contains many triggers that fire on high-p_T muon candidates. The second stream we use consists generally of triggers that fire on varying amounts of missing transverse energy ($\not\!\!E_T$), generally above 30 GeV. The two independent streams together make up an inclusive trigger selection, in that an event can enter the analysis on *any* trigger in either of these two streams. The efficiency of data events in the muon ($\not\!\!E_T$) trigger set is measured in a data sample collected in the $\not\!\!E_T$ (muon) trigger collection. This trigger efficiency is parameterized with a NN, as a function of kinematic observables, and applied in the background modeling procedure.

We search for events with two muons consistent with the decay of a Z boson. We make several preliminary cuts on events containing muon candidate objects to reduce complications in processing the large data sets. These cuts include requiring transverse momentum $p_T > 10$ GeV/c, energy deposits

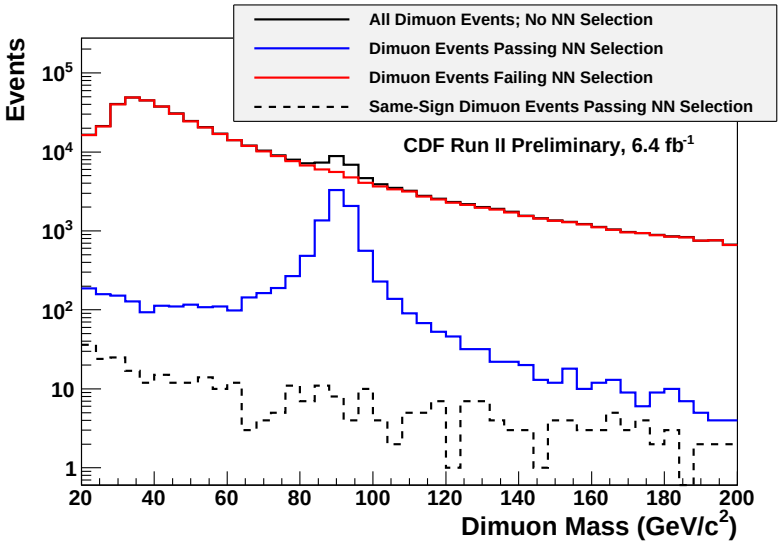

Figure 2: The distribution of dimuon mass for all events (black line), events passing the muon NN selection (blue), events failing the selection (red), and fake dimuon (QCD) events passing the muon NN selection (black dashed). The efficiency of the muon NN is high, while simultaneously maintaning a high rate of background rejection.

in the electromagnetic and hadronic calorimeters of no more than 4 GeV and 12 GeV, respectively, and the impact parameter of the track to be less than 0.2 cm from the primary vertex position. For all events, we require that the primary vertex position of the event is within 60 cm of the center of the detector.

The final muon candidate selection is done with a multivariate function which is trained to identify high-quality muon candidates and distinguish them from the fake muons arising in QCD production. This muon neural network (muon NN) is trained on single muons, allowing it to possibly be extended to other analyses which utilize high-p_T muons. The muon NN is trained using muons from a ZH Monte Carlo simulation as signal, and muons coming from same-sign dimuon events as background. The same-sign dimuon events are chosen since they are enriched in the QCD fake muon background.

The muon NN uses several kinematic properties of the muons as input variables: the energy deposits of the muon candidate in both the electromagnetic and hadronic calorimeters, the number of hits corresponding to the muon candidate track in the tracking chamber, the number of silicon hits corresponding to the track, the isolation of the muon candidate, the impact parameter and the χ^2 of the track, the η and ϕ position of the reconstructed muon object, as well as the minimum $\Delta R \equiv \sqrt{\Delta\eta^2 + \Delta\phi^2}$ between the muon candidate and the jets in the event.

We evaluate the muon NN for each candidate and require two muons to pass the muon NN requirements. Figure 2 shows the distribution of $m_{\mu\mu}$ for events both before and after the muon NN selection. The fake rate with the muon NN selection remains low, at about 4%.

Subsequent to finding two muons consistent with a Z boson ($76 < m_{\mu\mu} < 106$ GeV/c^2), we also require events have two or more jets, with $E_T > 15$ GeV. The lead jet in the event is required to have $E_T > 25$ GeV. All jets are required to be in the $|\eta| < 2$ region of the detector.

We apply the same neural network-derived jet energy corrections as previous CDF ZH analyses [7]. This correction improves the dijet mass resolution by assigning any missing transverse energy ($\not\!\!E_T$) back to the jets in the event based on projections of the $\not\!\!E_T$ on to individual jets. Since dijet mass is one of the most sensitive quantities to Higgs discrimination, this correction process enhances our sensitivity to Higgs production.

Events containing a good Z boson plus two or more jets satisfying the above criteria form the 'pre-tag' region of the analysis. This high-statistics region serves to validate the kinematic modeling of various background processes before moving on to the analysis of the signal region.

From the pre-tag selection, we apply further criteria to obtain the signal region used to produce the final results. We require one or more of the selected jets to be b-tagged, meaning the jet is likely to come from the production and resulting hadronization of a b quark. Two different b-tagging algorithms are used in this analysis. The secondary vertex (SecVtx) algorithm [8] assigns b-tags to jets by searching for tracks which have vertices displaced from the original interaction vertex. The SecVtx algorithm has two separate qualities - tight and loose, with the tight SecVtx b-tag being the better of the two. We also use the jet probability (JP) algorithm [9]. The JP algorithm assigns a probability for the given jet to originate from the interaction vertex. Therefore, b-jets will have lower JP probabilities.

Using the three b-tagging algorithms mentioned above, we define three tag categories to use in this analysis, each of which as a different signal-to-background ratio. First we search for two or more jets having a tight SecVtx tag. This double tag (DT) category contains the highest purity of ZH signal. If this is not the case, we search for one jet to have a loose SecVtx tag and another to have a JP tag (L+JP). The third and final tag category requires that only one of the jets have a tight SecVtx tag (ST). These three b-tagged categories (ST, L+JP, and DT) of events make up the signal region for this analysis.

3 Background Model

The main background consists of events with a Z boson (we include the small component due to $Z \to \tau\tau$ decays) and additional jets from QCD production. This background includes both light flavor (u, d, s, g) and heavy flavor jets (b, c). The Z+heavy flavor jets contribute most in the tag categories, while most of the Z+light jets background is removed by requiring tagged jets. The Z+jets background is modeled using ALPGEN [10], with PYTHIA [11] used to model the subsequent showering process. We apply a K-factor of 1.4 ± 0.4 to account for NLO effects.

To model the Z+light flavor jets background in the three tag categories, we do not use Monte Carlo samples as is done in the pre-tag region. Instead we use the pre-tag data sample in conjunction with a mistag matrix to estimate the actual rate of (mis-)tagged light flavor jets entering the final signal region. The mistag matrix is measured using dijet data events. Pre-tag data events are weighted according to this mistag matrix to obtain an expected number of b-tagged jets in the light flavor background. Since the pre-tag region is comprised mainly of Z+light flavor jets, this gives an accurate estimation of the rate of b-tags for light flavor jets.

There are other additional background processes that contribute to the analysis, but to a lesser degree. These backgrounds include diboson production (ZZ, WZ, WW) and $t\bar{t}$ production, and are modeled using PYTHIA alone.

The final category of background events includes fake $Z \to \mu\mu$ decays. This background is modeled using same-sign dimuon events from data, with the same $m_{\mu\mu}$ requirement. The two muons having the same charge are both required to pass the muon NN selection as outlined above. Because the contribution of fake events is small in the three tag categories, to model this we use the shape of $\mu^{\pm}\mu^{\pm}$ events in the pre-tag region, and scale this shape to the actual rate of same-sign dimuon events observed in each of the three tag categories.

Table 1 shows the expected number of events at the pre-tag level of the analysis for each background process, as well as the observed number of data events. The observed and expected event yields are well within uncertainties. Figures 3 and 4 show some kinematic distributions at the pre-tag level, to validate the analysis selection.

Process	**Expected Events**		
$Z + q\bar{q}$	10771.0	$\pm$	2154.2
$Z \to \mu\mu + c\bar{c}$	745.9	$\pm$	298.4
$Z \to \mu\mu + b\bar{b}$	406.9	$\pm$	162.7
$t\bar{t}$	86.7	$\pm$	8.7
ZZ	128.9	$\pm$	15.1
WZ	116.6	$\pm$	7.0
WW	5.5	$\pm$	0.3
Fake $Z \to \mu\mu$	502	$\pm$	25.1
Total Background	12763.5	$\pm$	2181.1
Observed Data	12853		
Expected ZH_{115} Signal	5.68	$\pm$	0.60

Table 1: Event yields for this analysis, prior to the application of b-tagging. This pre-tag region serves to validate the analysis framework. Expected ZH signal is shown, for $m_H = 115$ GeV/c^2.

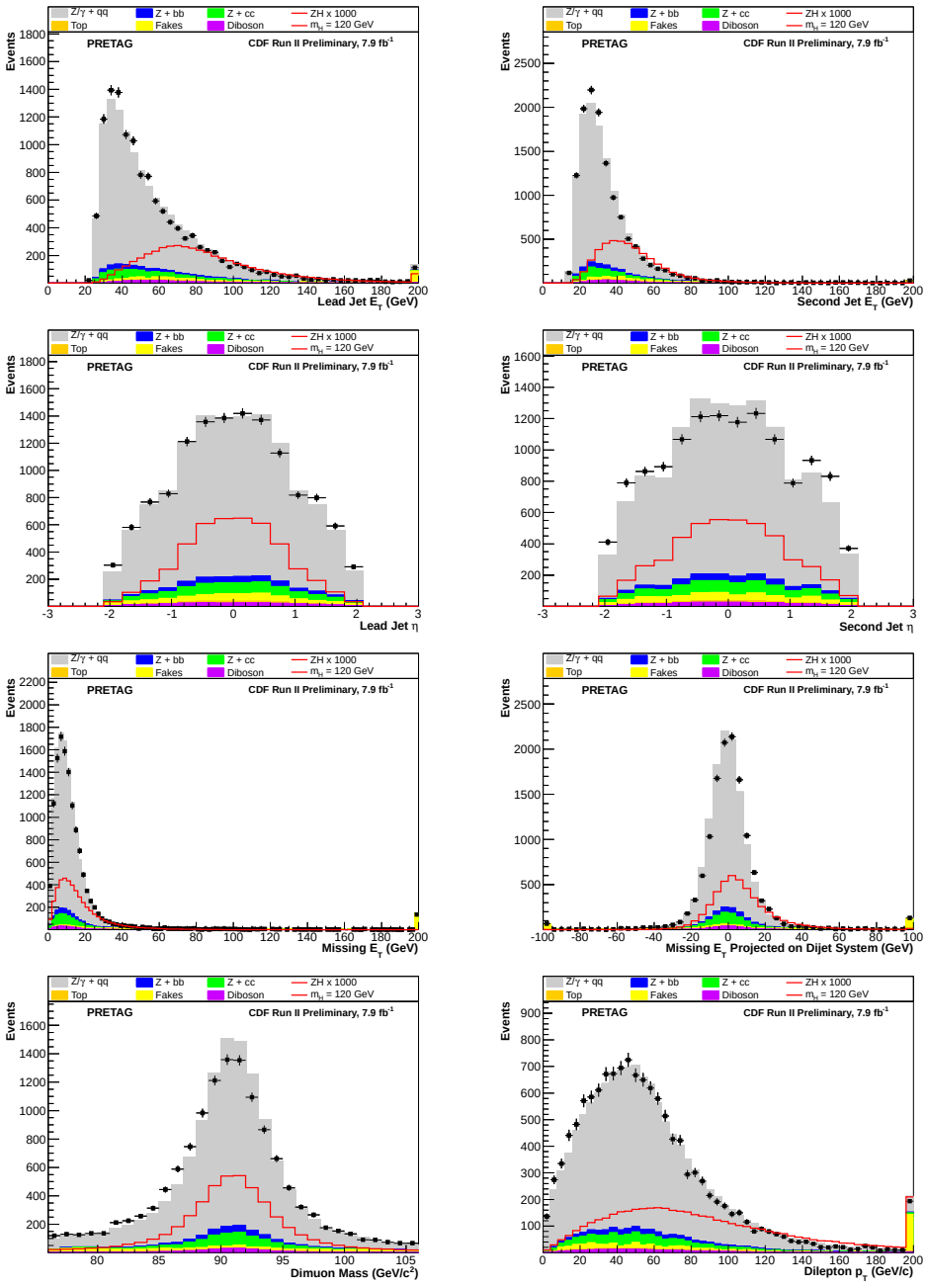

Figure 3: Several kinematic distributions to compare the background model used in this analysis with the observed data events. Systematic uncertainties on the total background model are shown with the hatched bands.

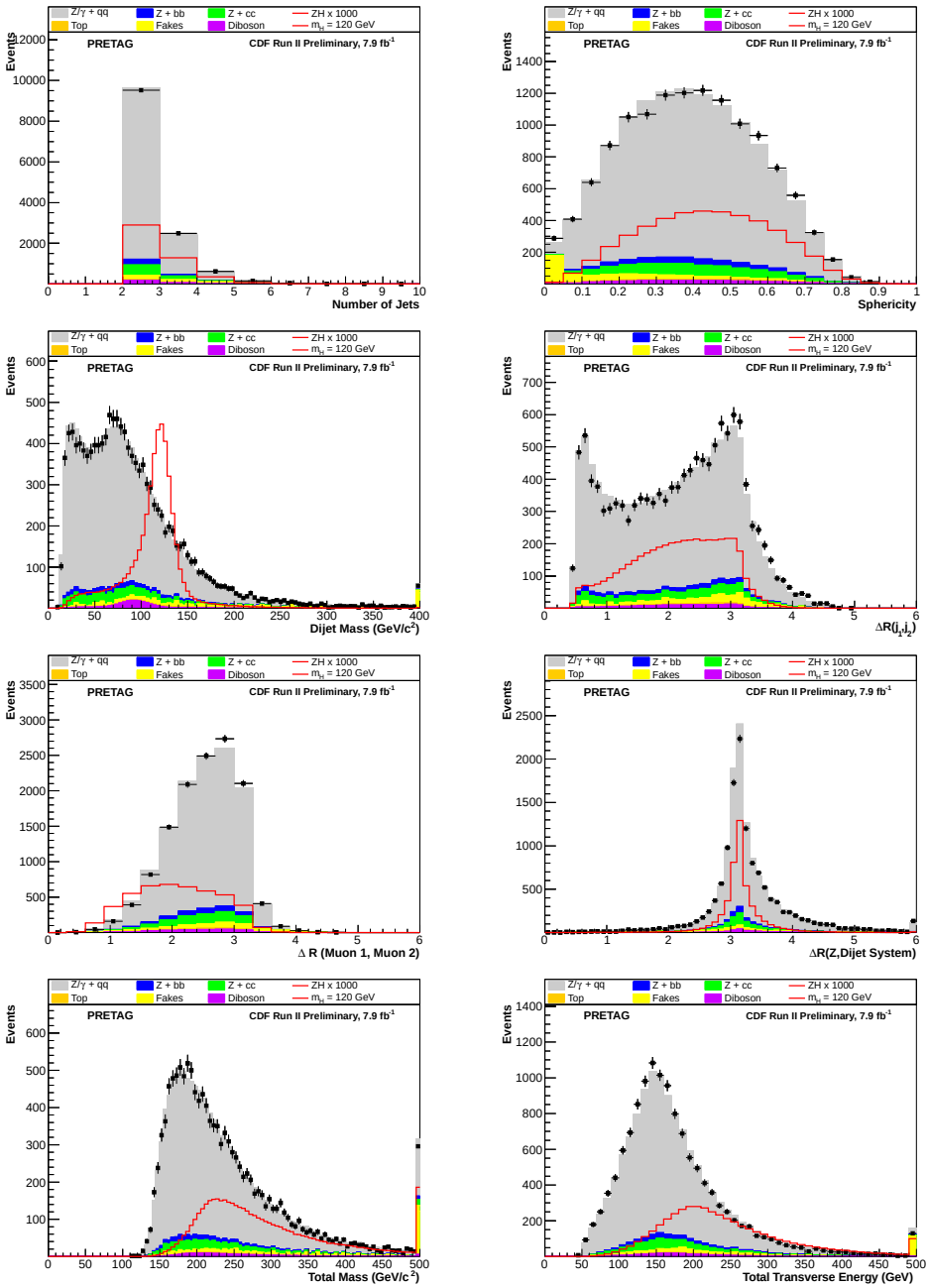

Figure 4: Several kinematic distributions to compare the background model used in this analysis with the observed data events. Systematic uncertainties on the total background model are shown with the hatched bands.

Expected $ZH \to \mu\mu b\bar{b}$ Events in 7.9 fb^{-1}

Higgs Mass (GeV/c^2)	Pre-Tag	ST	L+JP	DT
100	8.90	2.98	1.17	0.97
105	7.75	2.58	1.02	0.87
110	6.69	2.22	0.90	0.76
115	5.68	1.90	0.77	0.66
120	4.64	1.55	0.63	0.53
125	3.75	1.25	0.51	0.44
130	2.89	0.97	0.40	0.33
135	2.13	0.71	0.29	0.25
140	1.50	0.50	0.21	0.17
145	1.00	0.33	0.14	0.12
150	0.61	0.20	0.09	0.07

Table 2: Expected $ZH \to \mu\mu b\bar{b}$ events for this analysis, for the three tag categories as well as the pre-tag region.

Process **Expected Events**	ST	L+JP	DT
$Z \to \mu\mu+$ Mistags	207.4 ± 28.0	19.3 ± 4.8	1.2 ± 0.2
$Z \to \mu\mu + c\bar{c}$	57.8 ± 23.1	9.5 ± 3.8	1.6 ± 0.6
$Z \to \mu\mu + b\bar{b}$	117.4 ± 47.0	26.2 ± 10.5	17.3 ± 6.9
$t\bar{t}$	26.7 ± 2.7	11.7 ± 1.2	9.8 ± 1.0
ZZ	11.0 ± 0.7	3.5 ± 0.2	2.4 ± 0.1
WZ	3.9 ± 0.2	0.3 ± 0.01	
WW	0.2 ± 0.01		
Misidentified $Z \to \mu\mu$	21 ± 1.1	3 ± 0.2	0
Total Background	445.4 ± 59.4	73.6 ± 12.2	32.3 ± 7.0
Observed Data	450	73	34
Expected ZH_{115} Signal	1.90 ± 0.20	0.77 ± 0.08	0.66 ± 0.07

Table 3: Event yields for the three tagging categories used in this analysis. Expected ZH signal is shown, for $m_H = 115$ GeV/c^2.

After validating the analysis in the pre-tag region, we move to looking at the three tag categories which comprise the signal region of the analysis. The expected number of events and observed data in each category is shown in Table 3. Table 2 shows the expected number of $ZH \to \mu\mu b\bar{b}$ events expected in the pre-tag and tag regions of this analysis, for each mass point.

4 Multi-Layer Signal Discriminants

A new feature to this iteration of the CDF II $ZH \to \ell^+\ell^- b\bar{b}$ analysis is the use of a multi-layer discriminant technique, utilizing expert discriminants. Previous iterations of this analysis ([7], [12]) have used a two-dimensional final discriminant which simultaneously separates the Z+jets and $t\bar{t}$ backgrounds from the ZH signal events. In the multi-layer approach, we keep the ability to simultaneously separate these two classes of background while maintaning high signal purity. In addition, the process of combining this analysis result with others is made more simple after moving to a one-dimensional final discriminant approach.

The first step in this multi-layer approach is to train a signal discriminant, in the usual way. For our signal discriminants, we train using ZH events and a background sample composed of each different

background process contributing to the final signal region. The ZH signal sample is generated using PYTHIA [11], with forced $Z \to \ell^+\ell^-$ and $H \to b\bar{b}$ decays. A different signal discriminant is trained for each Higgs mass hypothesis used in the analysis, $100 < m_H < 150$ GeV/c^2 in steps of 5 GeV/c^2. This gives a total of 11 independent discriminants trained for each individual Higgs mass point.

The signal discriminants are trained using several kinematic variables, which are listed here:

- $\not\!\!E_T$ — The missing energy in the event, corrected for jets and muons.
- n_{jet} — The number of tight jets in the event.
- $\vec{\not\!\!E_T} \cdot (\vec{j_1} + \vec{j_2})$ — The projection of the $\not\!\!E_T$ vector on to the vector sum of the two leading jets in the event.
- $P_T(Z)$ — The transverse momentum of the reconstructed Z boson.
- $P_T(j_1 + j_2)$ — The transverse momentum of the dijet system.
- $\sum E_T$ — The scalar sum of the E_T of the Z and all tight jets in the event.
- m_{jj} — The dijet mass (or reconstructed Higgs boson mass).
- $\Delta R_{j_1,j_2}$ — The separation between the lead and secondary jet.
- $\Delta R_{Z,j_1j_2}$ — The separation between the reconstructed Z and dijet system.
- $\Delta R_{\mu_1,\mu_2}$ — The separation between the two muons in the event.
- Sphericity — An angular measure which takes into account the distribution of all reconstructed objects and their positions in the detector.
- m_{Tot} — The total mass of all reconstructed objects (2 leptons and all jets).
- m_{Zjj} — The total reconstructed mass of the Z boson, lead, and secondary jets in the event.
- $p_T(\mu_i)$ — The transverse momentum of each of the two muons in the event.

Additionally, for the signal discriminants we use an ensemble of networks. Each mass point has ~ 50 networks trained independently, and each event is sent through each of the networks comprising the ensemble. The output score for that event is simply the average over all of the constituent networks in the ensemble. It has been observed that this method reduces fluctuations in the observed limits, due to the choice of random seeding in the training process.

Once the signal discriminants are trained, we can enhance signal discrimination through the multi-layer method. The first step is to utilize an expert discriminant trained to separate $t\bar{t}$ events from Z+jets events. The output of this expert discriminant is shown in Figure 5. We make a cut on this discriminant output to define a $t\bar{t}$-rich region, similar to the behaviour of one corner in the two-dimensional network used in previous versions of this analysis.

After defining the $t\bar{t}$-rich region, we apply a second expert discriminant to further enhance the signal purity of events falling into specific bins of the output discriminant. In this second step, we use the Karlsruhe flavor separator function (KIT) [13], which attempts to separate b-jets from c-jets and light flavor jets. Since we expect a $H \to b\bar{b}$ decay, separating the Z+light and Z+charm backgrounds can be very beneficial to the sensitivity of the analysis. Figure 6 shows the output of the KIT flavor separator for $Z + b\bar{b}$ and $Z + c\bar{c}$ events, which are very well separated. A cut on the output of this function defines a b-enriched region and a light flavor and charm enriched region.

After sending each event through this multi-layer decision process, we obtain a final event discriminant consisting of three regions: a $t\bar{t}$ rich region from 0 to 1, a light flavor-enriched region from 1 to 2 (this region also contains most $Z + c\bar{c}$ events, and a heavy-flavor region from 2 to 3, where we expect most ZH signal events to fall. Figure 7 shows the final discriminant output which was trained specifically for a Higgs boson with mass 120 GeV/c^2. The three regions can clearly be seen, however, the effect becomes more substantial when looking at the three tag categories used as the signal region for this analysis.

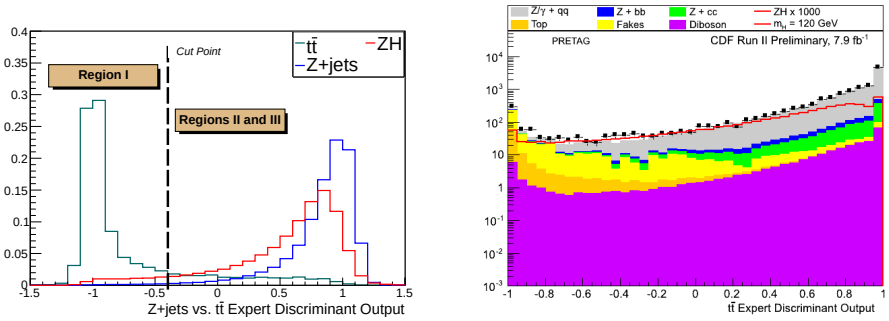

Figure 5: The $t\bar{t}$ vs. Z+jets expert discriminant

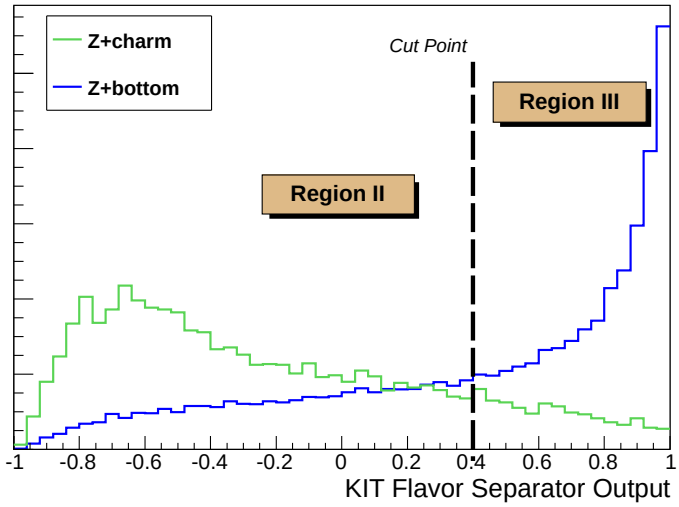

Figure 6: The KIT flavor separator output for $Z + b\bar{b}$ (blue) events and $Z + c\bar{c}$ (green) events.

After describing the method used to produce final discriminant outputs, we show the input variable kinematic distributions for each of the three tag categories used in the analysis. These can be seen in Figures 8, 9, and 10.

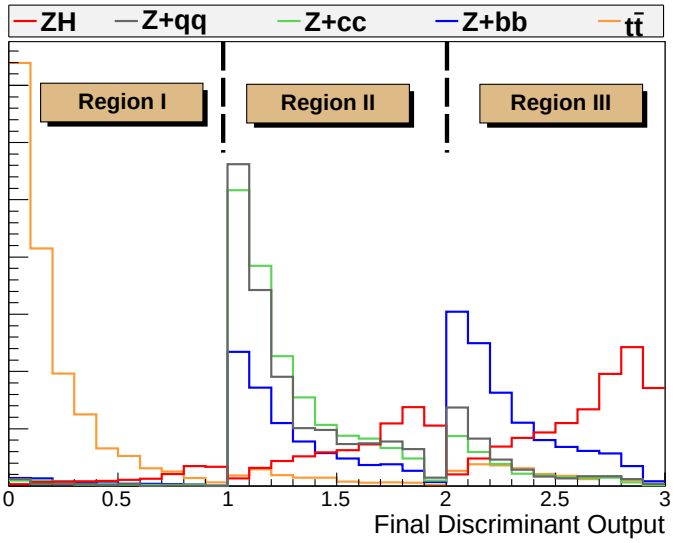

Figure 7: The final discriminant outputs for each main class of background, and signal events, at pre-tag level, for a Higgs mass of 120 GeV/c^2. These shapes are drawn normalized to unit area to show the behavior of the multi-layer discriminant method.

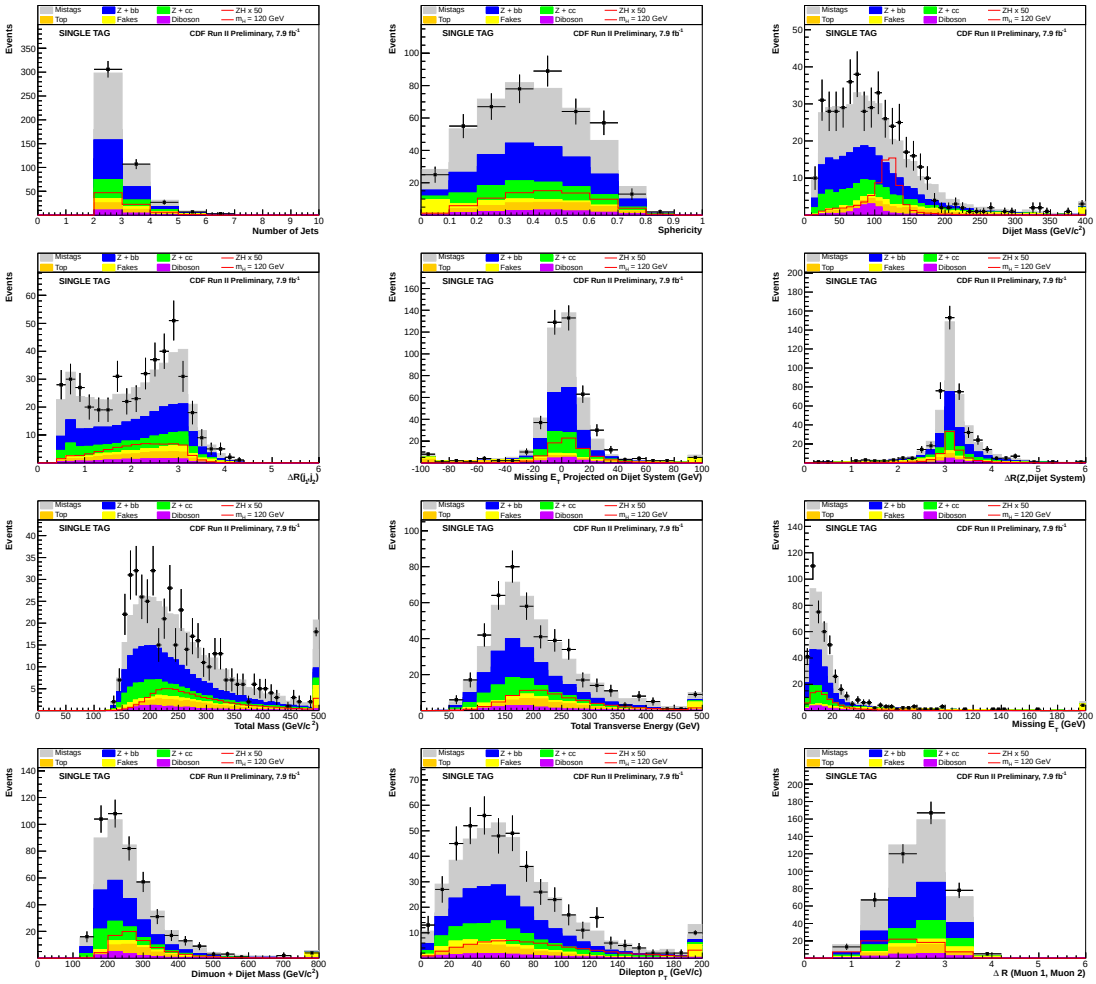

Figure 8: Final event discriminant inputs for the single tight SecVtx b-tagging category.

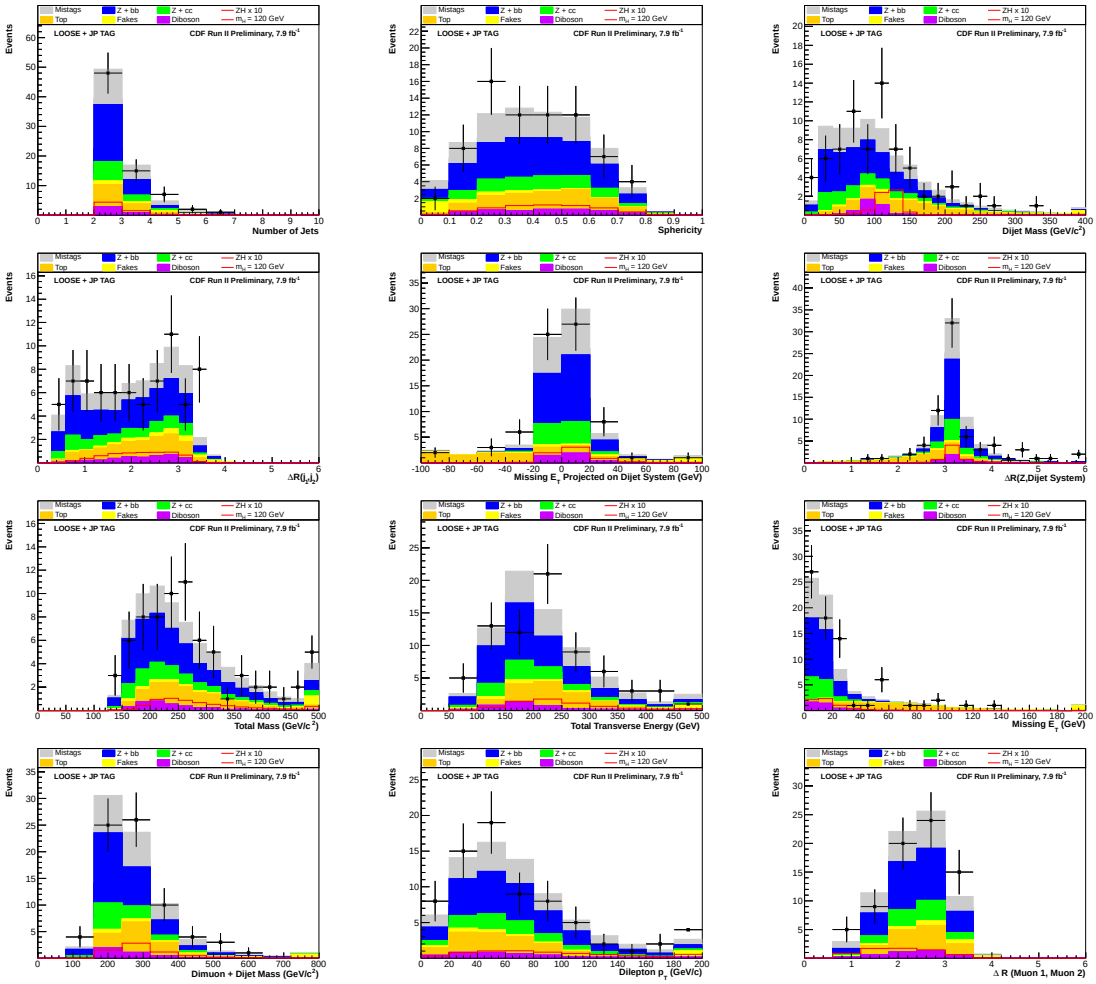

Figure 9: Final event discriminant inputs for the loose SecVtx + jet probability b-tagging category.

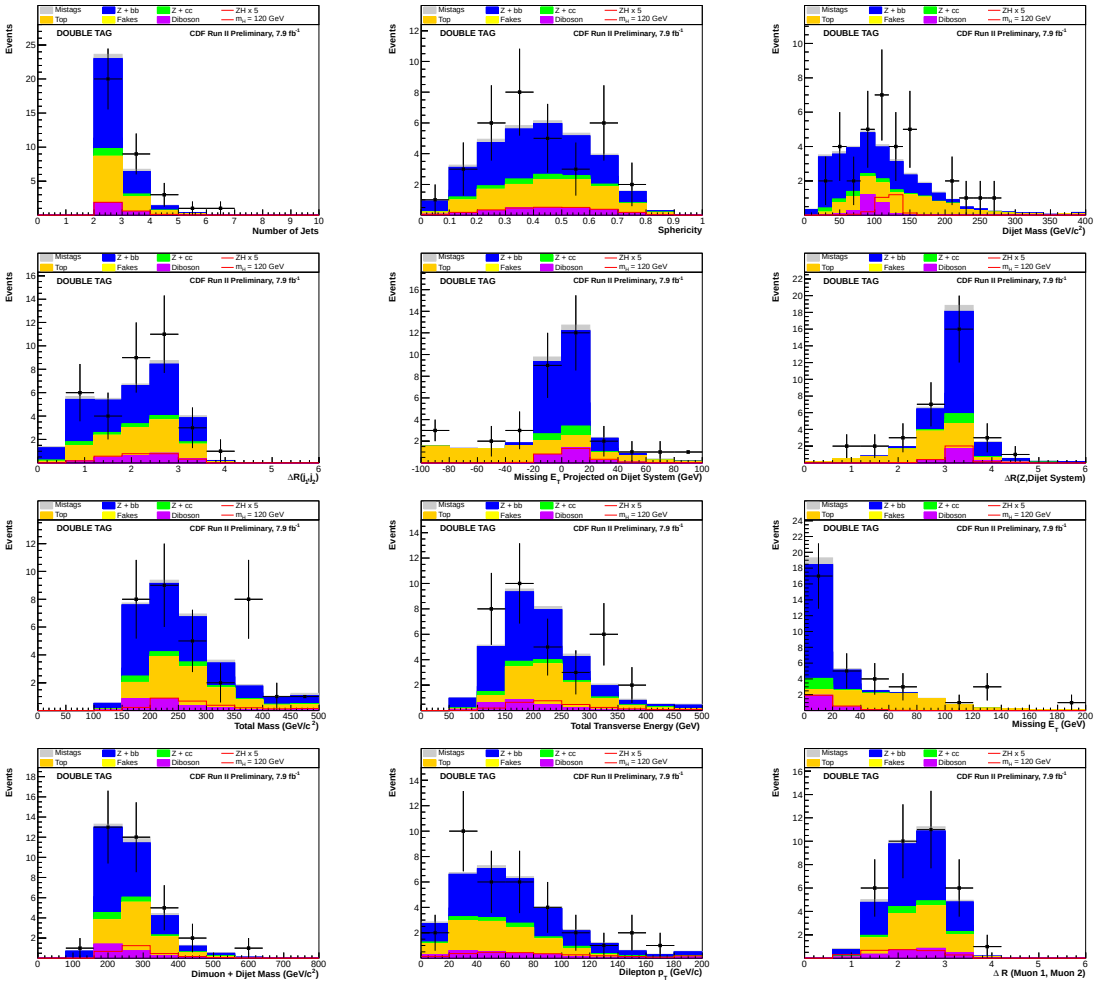

Figure 10: Final event discriminant inputs for the double tight SecVtx b-tagging category.

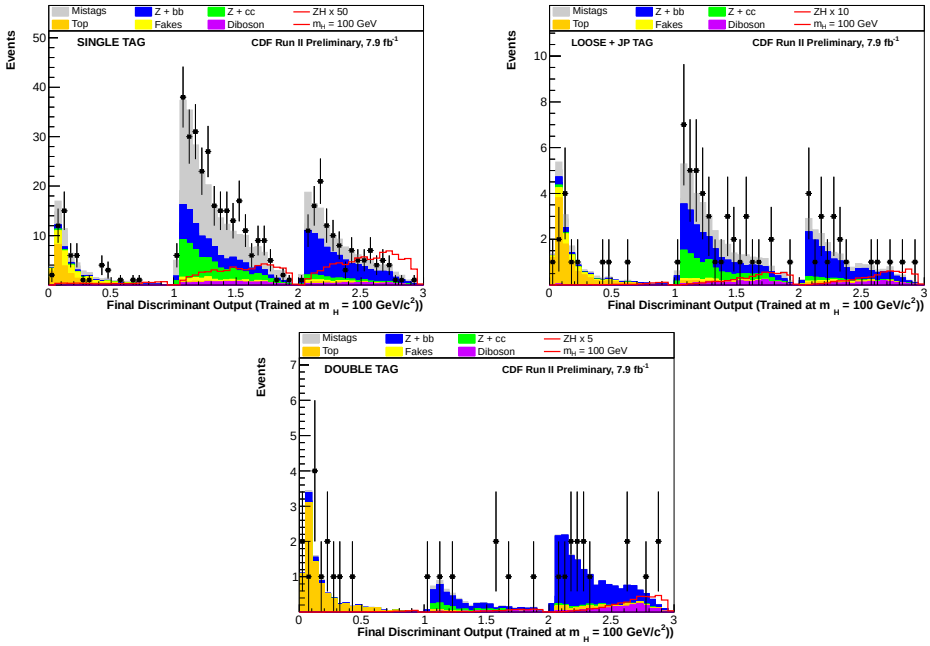

Figure 11: Final discriminant outputs for each tag category, for $m_H = 100$ GeV/c^2.

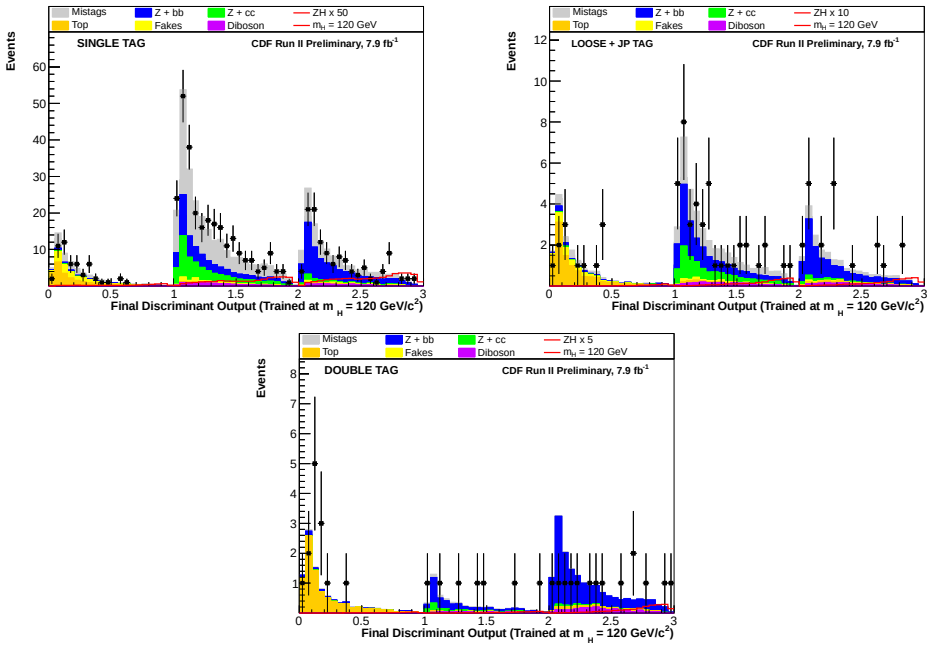

Figure 12: Final discriminant outputs for each tag category, for $m_H = 120$ GeV/c^2.

We next show the final output discriminants for a few Higgs mass hypotheses, for each of the tag categories. Figure 11 shows the output for $m_H = 100$ GeV/c^2. Figure 12 shows the output for $m_H = 120$ GeV/c^2, while figure 13 shows the output for $m_H = 150$ GeV/c^2.

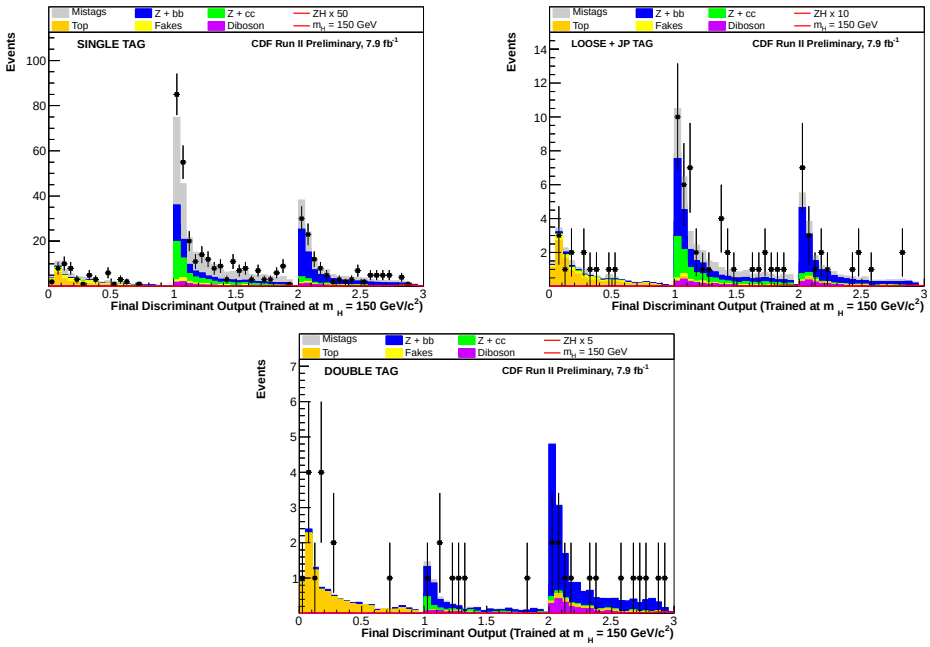

Figure 13: Final discriminant outputs for each tag category, for $m_H = 150$ GeV/c^2.

CDF $ZH \to \mu\mu b\bar{b}$ Analysis — Single Tag (ST) Category							CDF Run II Preliminary, 7.9 fb^{-1}
Contribution	Fakes	$t\bar{t}$	WW, WZ, ZZ	$Z + b\bar{b}$	$Z + c\bar{c}$	Mistags	ZH
Luminosity ($\sigma_{\text{inel}}(p\bar{p})$)		3.8	3.8	3.8	3.8		3.8
Luminosity Monitor		4.4	4.4	4.4	4.4		4.4
Lepton ID		1	1	1	1		1
Lepton Energy Scale		1.5	1.5	1.5	1.5		1.5
Fake Leptons	5						
Mistag Rate						$^{+13.5}_{-13.6}$	
Jet Energy Scale (shape dep.)		$^{+1.8}_{-1.9}$	$WW^{+18.7}_{-3.7}$, $WZ^{+3.9}_{-4.3}$, $ZZ^{+4.3}_{-5.4}$	$^{+7.9}_{-6.7}$	$^{+7.9}_{-6.6}$		$^{+1.6}_{-2.6}$
b-tag Rate		5.2	5.2	5.2	5.2		5.2
$t\bar{t}$ Cross Section		10					
Diboson Cross Section			6				
Z+HF Cross Section				40	40		
ZH Cross Section							5
ISR/FSR							1
NN Trigger Model		5	5	5	5		5

CDF $ZH \to \mu\mu b\bar{b}$ Analysis — Loose + JetProb (LJP) Category							CDF Run II Preliminary, 7.9 fb^{-1}
Contribution	Fakes	$t\bar{t}$	WW, WZ, ZZ	$Z + b\bar{b}$	$Z + c\bar{c}$	Mistags	ZH
Luminosity ($\sigma_{\text{inel}}(p\bar{p})$)		3.8	3.8	3.8	3.8		3.8
Luminosity Monitor		4.4	4.4	4.4	4.4		4.4
Lepton ID		1	1	1	1		1
Lepton Energy Scale		1.5	1.5	1.5	1.5		1.5
Fake Leptons	5						
Mistag Rate						$^{+27.2}_{-24.0}$	
Jet Energy Scale (shape dep.)		$^{+1.6}_{-1.8}$	$WW^{+3.5}_{-3.7}$, $WZ^{+4.6}_{-7.6}$, $ZZ^{+4.0}_{-4.2}$	$^{+6.9}_{-5.9}$	$^{+7.8}_{-5.9}$		$^{+1.5}_{-2.3}$
b-tag Rate		8.7	8.7	8.7	8.7		8.7
$t\bar{t}$ Cross Section		10					
Diboson Cross Section			6				
Z+HF Cross Section				40	40		
ZH Cross Section							5
ISR/FSR							2
NN Trigger Model		5	5	5	5		5

CDF $ZH \to \mu\mu b\bar{b}$ Analysis — Double Tag (DT) Category							CDF Run II Preliminary, 7.9 fb^{-1}
Contribution	Fakes	$t\bar{t}$	WZ, ZZ, WW	$Z + b\bar{b}$	$Z + c\bar{c}$	Mistags	ZH
Luminosity ($\sigma_{\text{inel}}(p\bar{p})$)		3.8	3.8	3.8	3.8		3.8
Luminosity Monitor		4.4	4.4	4.4	4.4		4.4
Lepton ID		1	1	1	1		1
Lepton Energy Scale		1.5	1.5	1.5	1.5		1.5
Fake Leptons	5						
Mistag Rate						$^{+28.7}_{-25.1}$	
Jet Energy Scale (shape dep.)		$^{+1.6}_{-1.7}$	$WW^{+3.5}_{-3.7}$, $WZ^{+3.5}_{-3.7}$, $ZZ^{+4.1}_{-4.4}$	$^{+7.5}_{-3.8}$	$^{+6.6}_{-5.2}$		$^{+1.4}_{-2.3}$
b-tag Rate		10.2	10.2	10.2	10.2		10.2
$t\bar{t}$ Cross Section		10					
Diboson Cross Section			6				
Z+HF Cross Section				40	40		
ZH Cross Section							5
ISR/FSR							5
NN Trigger Model		5	5	5	5		5

Table 4: Systematic uncertainties on the analysis. Systematic uncertainties for $ZH \to \mu\mu b\bar{b}$ shown in this table are obtained for $m_H = 120$ GeV/c^2. Uncertainties are relative, in percent, and are symmetric unless otherwise indicated.

5 Systematics

We apply several systematic errors to this analysis to account for theoretical and experimental uncertainties. The majority of these systematics are rate uncertainties, such as theoretical errors on predicted cross sections. Other systematics are due to detector effects, such as lepton selection and reconstruction efficiency, as well as measurement of the luminosity.

Because of differences in applying the b-tag algorithms to Monte Carlo and data, we apply a scale factor to the Monte Carlo events in the tag categories. There is a systematic uncertainty on this factor, known as the b-tag scale factor uncertainty. It depends on the specific combinations of tag algorithms used in each tag category.

Apart from the various rate uncertainties described above, there are additional systematics which affect the shape of the final event discriminants. These shape uncertainties include effects due to the jet energy scale, as well as production of initial or final state radiation. The mistag event weights also contribute an additional shape uncertainty.

Table 4 shows the various systematic uncertainties applied to each Monte Carlo or data-derived background. The numbers shown are percent uncertainties, and are symmetric unless otherwise indicated. These numbers are obtained for the $m_H = 120$ GeV/c^2 mass point.

m_H (GeV/c^2)	Observed Limit	Expected Limits				
		-2σ	-1σ	Median	+1σ	+2σ
100	**6.2**	2.6	3.4	**4.8**	6.9	9.5
105	**7.6**	2.8	3.6	**5.1**	7.2	10.2
110	**8.8**	3.0	4.1	**5.6**	8.2	11.3
115	**10.2**	3.3	4.3	**6.0**	8.6	12.3
120	**12.8**	4.0	5.2	**7.4**	10.1	14.1
125	**13.4**	4.5	6.0	**8.5**	12.2	17.6
130	**18.9**	5.8	7.7	**11.0**	15.9	23.3
135	**22.7**	7.7	10.4	**14.8**	20.8	29.5
140	**26.7**	11.0	14.2	**19.7**	28.1	40.1
145	**36.6**	16.0	20.8	**28.5**	41.2	54.2
150	**51.8**	24.6	33.3	**44.8**	64.3	95.0

Table 5: Observed and expected limits, for all tagging categories combined. The observed limits include the $\pm 1\sigma$ and $\pm 2\sigma$ error values as well.

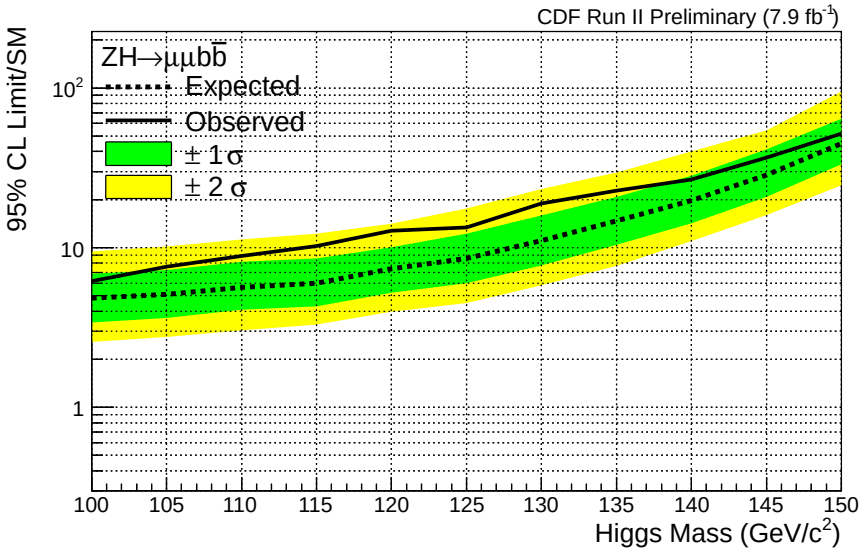

Figure 14: Expected limits for this analysis, shown in the dotted line. The solid line shows the observed limits.

6 Results

After performing the search for $ZH \to \mu^+\mu^- b\bar{b}$ events in the three tag categories described above, we do not observe an excess that would be consistent with the ZH signal, and proceed to set upper limits on the Higgs boson production cross section times $H \to b\bar{b}$ branching ratio. To do this we use the software package MCLimit [14], which utilizes many pseudoexperiment samplings of the statistical and systematic parameter space to obtain expected and observed limits.

The results, in the form of upper limits at the 95 percent confidence level, are shown in Table 5 and graphically in Figure 14.

7 Conclusion

We have performed a search for the Standard Model Higgs boson in the $ZH \to \mu^+\mu^- b\bar{b}$ final state using 7.9 fb^{-1} of integrated luminosity collected with the CDF II detector. We have implemented several new techniques in this iteration of the analysis, including the use of a multivariate function to select high-quality muons. The use of expert discriminants in the multi-layer signal discriminant method proved to be very useful in enhancing signal purity in the final signal regions of the analysis. We plan to combine this result with the $ZH \to e^+e^- b\bar{b}$ analysis, and additionally this analysis will be part of the Tevatron Higgs combination results for Summer 2011 conferences.

References

[1] Peter W. Higgs, Broken Symmetries and the Masses of Gauge Bosons. Phys. Rev. Lett. **13**, 508 (1964).

[2] The LEP Working Group for Higgs Boson Searches, Search for the Standard Model Higgs boson at LEP. Phys. Lett. B **565**, 61-75 (2003).

[3] Combined CDF and D0 Upper Limits on Standard Model Higgs Boson Production with up to 8.2 fb^{-1} of Data. `arXiv:1103.3233`

[4] Combined CDF and D0 Upper Limits on Standard Model Higgs-Boson Production with up to 6.7 fb^{-1} of Data. `arXiv:1007.4587`

[5] GSM - A Gfitter Package for the Global Electroweak Fit.
`http://project-gfitter.web.cern.ch/project-gfitter/GSM/`

[6] S. Lockwitz, et.al. A Search for the Standard Model Higgs Boson in the Process $ZH \to e^+e^- b\bar{b}$ Using 7.5fb^{-1} of CDF II Data. CDF Public Note 10593.

[7] The CDF Collaboration, A Search for the Standard Model Higgs Boson in the Process $ZH \to \ell^+\ell^- b\bar{b}$ Using 4.1 fb^{-1} of CDF II Data. CDF Public Note 9889.

[8] The CDF Collaboration, Measurement of the $t\bar{t}$ Production Cross Section in $p\bar{p}$ collisions at $\sqrt{s} =$ 1.96 TeV using Lepton + Jets Events with Secondary Vertex b-tagging. CDF Public Note 7138.

[9] Enrique Palencia, Measurement of the $t\bar{t}$ Production Cross Section in $p\bar{p}$ Collisions at $\sqrt{s} = 1.96$ TeV Using Lepton+Jets Events in the CDF Detector at Fermilab. Ph.D. Thesis, CDF Public Note 8772.

[10] M.L. Mangano, M. Moretti, F. Piccinini, R. Pittau, A.D. Polosa, ALPGEN, a generator for hard multiparton processes in hadronic collisions. `arXiv:hep-ph/0206293`.

[11] Torbjorn Sjostrand, Stephen Mrenna, Peter Skands, PYTHIA 6.4 Physics and Manual, `arXiv:hep-ph/0603175`.

[12] J. Pilot, et.al. A Search for the Standard Model Higgs Boson in the Process $ZH \to \mu^+\mu^- b\bar{b}$ Using a Loosened Muon Selection. CDF Public Note 10221.

[13] Svenja Richter, Search For Electroweak Single Top-Quark Production with the CDF II Experiment. PhD. Thesis, FERMILAB-THESIS-2007-35, November 2007

[14] Thomas Junk, Confidence Level Computation for Combining Searches with Small Statistics. `arXiv:hep-ex/9902006`.

Process **Expected Events**	ST	L+JP	DT
$Z \to \mu\mu+$ Mistags	185.4 ± 25.0	15.6 ± 4.4	1.0 ± 0.3
$Z \to \mu\mu + c\bar{c}$	52.7 ± 21.1	11.9 ± 1.2	1.5 ± 0.6
$Z \to \mu\mu + b\bar{b}$	107.1 ± 42.8	23.9 ± 9.5	15.8 ± 6.3
$t\bar{t}$	27.1 ± 2.7	11.9 ± 1.2	10.0 ± 1.0
ZZ	11.0 ± 0.7	3.5 ± 0.2	2.4 ± 0.1
WZ	3.9 ± 0.2	0.3 ± 0.01	
WW	0.2 ± 0.01		
Misidentified $Z \to \mu\mu$	21 ± 1.1	3 ± 0.2	0
Total Background	408.5 ± 54.0	66.9 ± 11.1	30.6 ± 6.4
Observed Data	450	73	34

Table 6: Event yields for the three tagging categories used in this analysis, prior to the MCLimit fit procedure.

A Plots Prior To Template Fit Procedure

As mentioned in Section 6, we use the MCLimit software package [14] to set the expected and observed limits on the Higgs production cross section times branching ratio. In the process of setting limits, a fit is performed. The software adjusts all of the background shapes within statistical and systematic fluctuations to form the 'best model' describing the data. It is from these post-fit distributions that the limits are set. In the main body of this note, we have shown the plots adjusted to the values fit by the MCLimit software. In figures 15, 16, and 17, we show the raw distributions that are given to MCLimit, prior to the fit procedure, for each of the three tag categories. Table 6 shows the event yields prior to this fitting procedure.

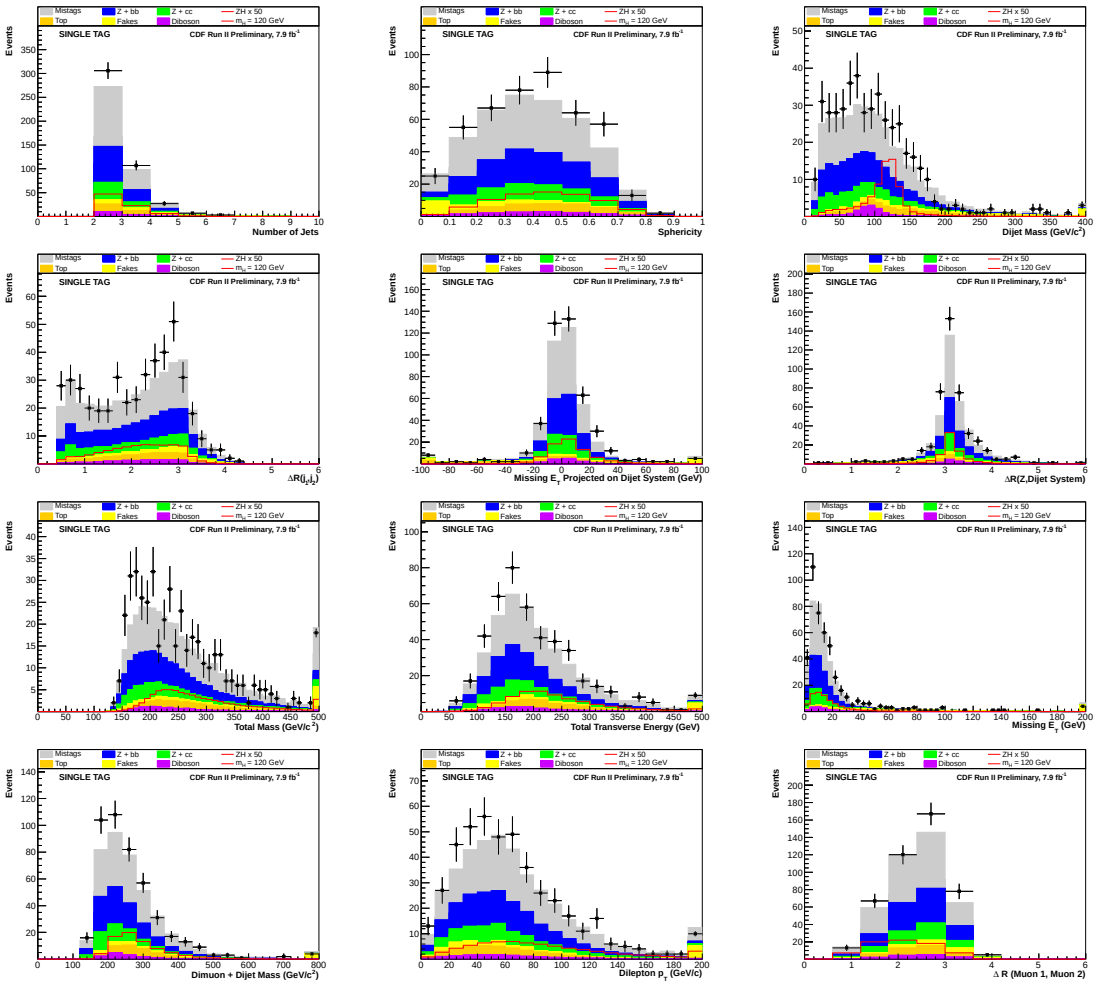

Figure 15: Final event discriminant inputs for the single tight SecVtx b-tagging category, prior to the MCLimit fit procedure.

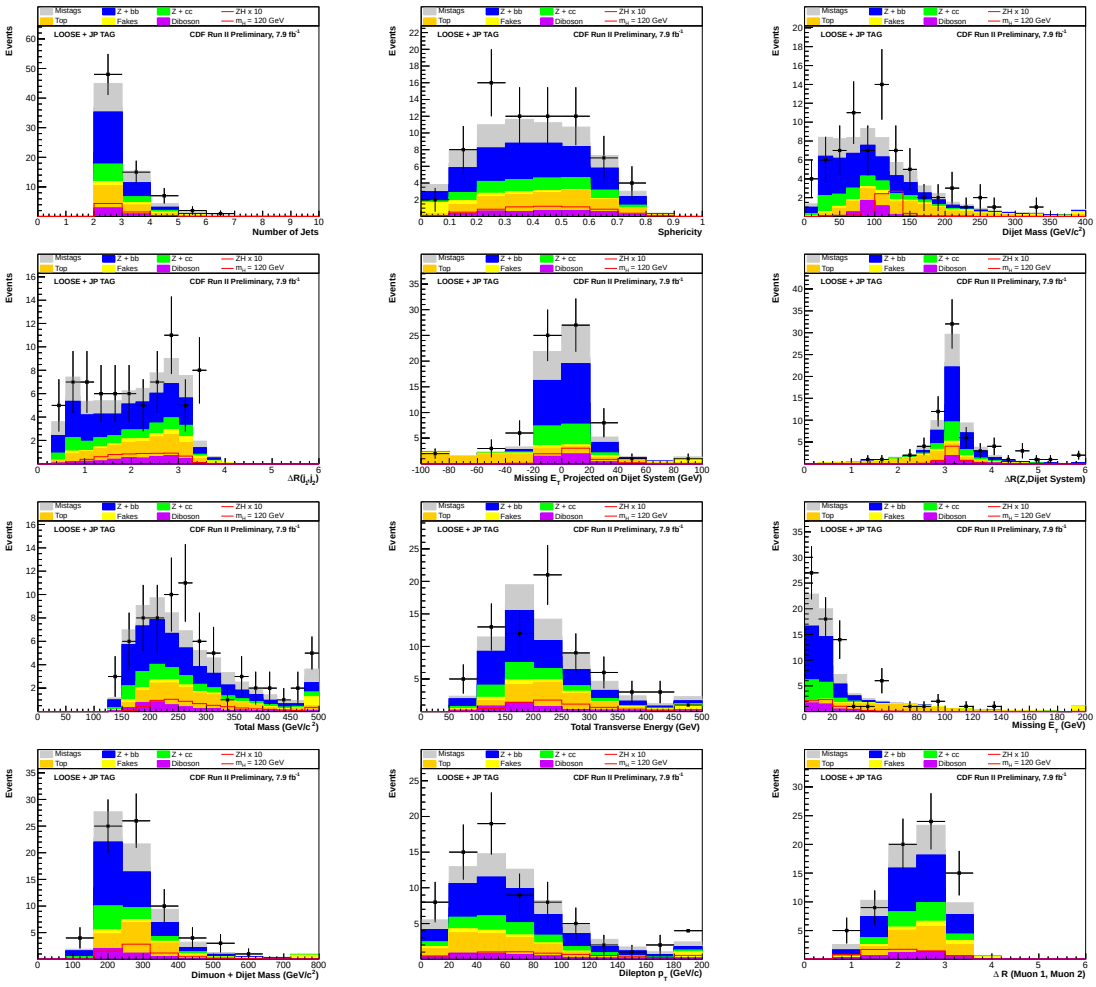

Figure 16: Final event discriminant inputs for the loose SecVtx + jet probability b-tagging category, prior to the MCLimit fit procedure.

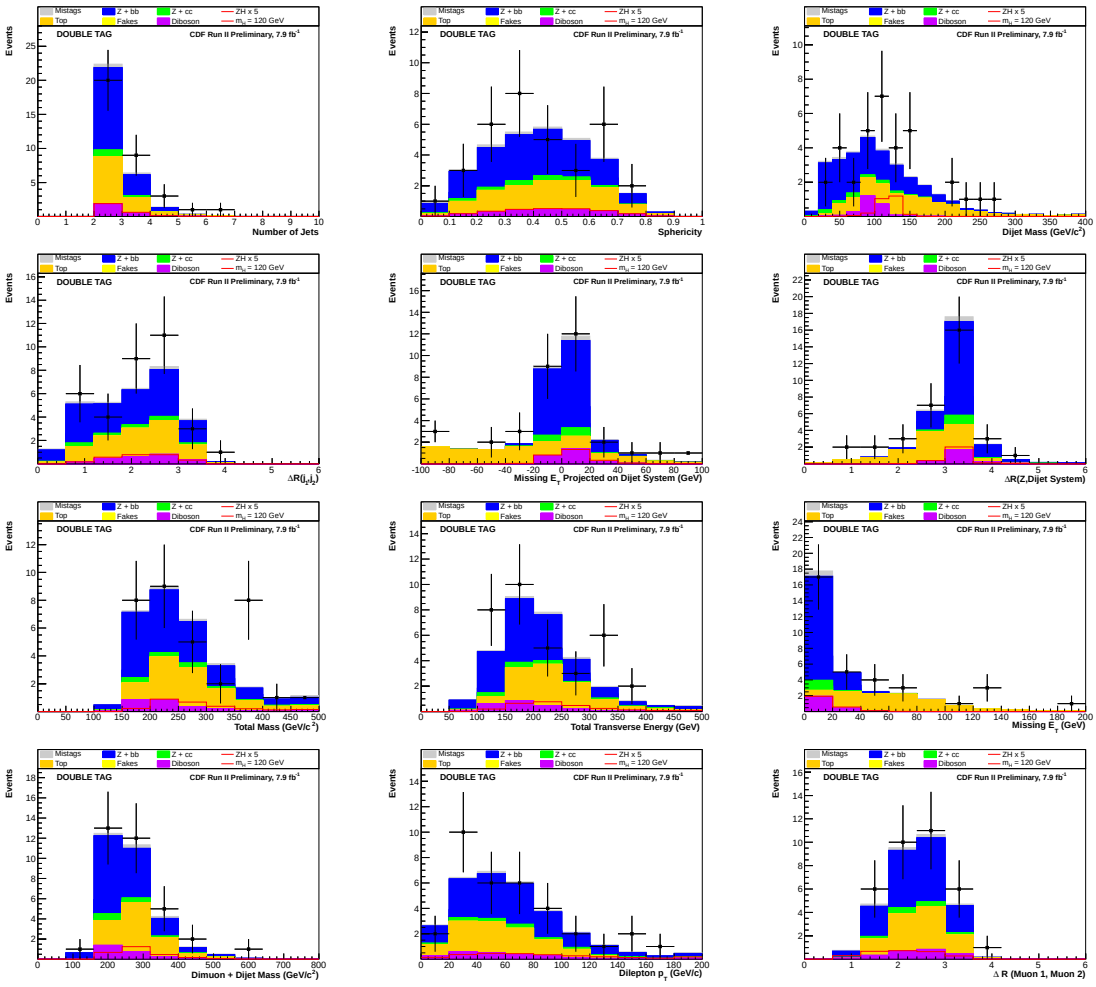

Figure 17: Final event discriminant inputs for the double tight SecVtx b-tagging category, prior to the MCLimit fit procedure.